**The EMBO Journal (2008) 27,** 2230–2238 | © 2008 European Molecular Biology Organization | All Rights Reserved 0261-4189/08
www.embojournal.org

THE EMBO JOURNAL

# Bacterial actin: architecture of the ParMRC plasmid DNA partitioning complex

**Jeanne Salje and Jan Löwe***

Structural Studies, MRC Laboratory of Molecular Biology, Cambridge, UK

**The R1 plasmid employs ATP-driven polymerisation of the actin-like protein ParM to move newly replicated DNA to opposite poles of a bacterial cell. This process is essential for ensuring accurate segregation of the low-copy number plasmid and is the best characterised example of DNA partitioning in prokaryotes. *In vivo*, ParM only forms long filaments when capped at both ends by attachment to a centromere-like region *parC*, through a small DNA-binding protein ParR. Here, we present biochemical and electron microscopy data leading to a model for the mechanism by which ParR–*parC* complexes bind and stabilise elongating ParM filaments. We propose that the open ring formed by oligomeric ParR dimers with *parC* DNA wrapped around acts as a rigid clamp, which holds the end of elongating ParM filaments while allowing entry of new ATP-bound monomers. We propose a processive mechanism by which cycles of ATP hydrolysis in polymerising ParM drives movement of ParR-bound *parC* DNA. Importantly, our model predicts that each pair of plasmids will be driven apart in the cell by just a single double helical ParM filament.**

*The EMBO Journal* (2008) **27,** 2230–2238. doi:10.1038/emboj.2008.152; Published online 24 July 2008
*Subject Categories*: cell & tissue architecture; cell cycle; structural biology
*Keywords*: actin; DNA segregation; ParM; ParR; plasmid partitioning

## Introduction

Accurate partitioning of DNA molecules during cell division is essential to ensure genetic stability. In eukaryotes, genome partitioning is achieved by employing force generated by microtubule dynamics and motor proteins. In contrast, chromosome segregation mechanisms in prokaryotes remain obscure (Sherratt, 2003; Ebersbach and Gerdes, 2005; Ghosh *et al*, 2006). Insight into one mechanism of prokaryotic DNA partitioning comes with the well-characterised R1 plasmid and its homologues (Gerdes *et al*, 2004). Plasmid R1 is a large (100 kb) low-copy number plasmid, which is stably maintained at 4–6 copies per cell (Nordström *et al*, 1980). The plasmid encodes a stability operon, *par*, which is both necessary and sufficient to confer stable partitioning. The R1 *par* operon encodes three components: ParM (StbA), ParR (StbB) and *parC* (Gerdes and Molin, 1986). ParM is a 37.5 kDa actin-like ATPase (Møller-Jensen *et al*, 2002), which characterises the operon as a type II plasmid-partitioning system (Gerdes *et al*, 2000). ParR is a 13.3 kDa DNA-binding protein, which binds cooperatively as a dimer to ten 11 bp repeats in the centromere-like *parC* DNA region (Dam and Gerdes, 1994; Møller-Jensen *et al*, 2003).

The current model for type II partitioning invokes ATP-driven polymerisation of ParM to push newly replicated plasmids to opposite poles of the cell (Møller-Jensen *et al*, 2003). ParM filaments are composed of two parallel protofilaments with a helical crossover distance and general appearance very similar to F-actin (van den Ent *et al*, 2002). Unlike actin, however, it is now clear that ParM assembles into left-handed filaments (Orlova *et al*, 2007; Popp *et al*, 2008). ParM exhibits dynamic instability in the presence of ATP, whereby both ends of the polar, double-helical protofilament undergo elongation followed by rapid disassembly (Garner *et al*, 2004). The presence of ParR and *parC* DNA protects the ParM filaments from disassembly and they grow into long and stable filaments (Garner *et al*, 2007). In the cell, it is thought that only when ParM filaments are capped by the ParR–*parC* complex at both ends, they are able to stably grow into long filaments and thereby push plasmids apart. ParR–*parC* complexes from R1, pB171 and pSK41 have recently been studied using X-ray crystallography and electron microscopy (Møller-Jensen *et al*, 2007; Schumacher *et al*, 2007) and shown to form a helical array of ParR dimers with *parC* DNA wrapped around the outside. pSK41 ParR was cocrystallised with short fragments of *parC* DNA (Schumacher *et al*, 2007), which bound around the outside of the ParR helix. *ParC* DNA wrapped around the outside of a ParR ring was also observed for R1 ParR using electron microscopy (Møller-Jensen *et al*, 2007). In both crystal structures, the C-terminal domains are either not present (pSK41; Schumacher *et al*, 2007) or disordered (pB171; Møller-Jensen *et al*, 2007). Fluorescence anisotropy experiments demonstrated that full-length ParR from pSK41 is required for interaction with ParM filaments (Schumacher *et al*, 2007).

The mechanism by which these helical ParR–*parC* protein DNA complexes stabilise ParM filaments is key to understanding type II plasmid partitioning and has remained elusive until now. Here, we have used a combination of biochemistry and electron microscopy to elucidate the architecture of ParR–*parC*-capped ParM filaments and to postulate a mechanism by which this stabilisation occurs. We propose that the open mouth of the ParR–*parC* helix structure forms a clamp around the end of elongating ParM filaments, and that each ParR–*parC* complex caps a single ParM protofilament.

*Corresponding author. Structural Studies, MRC Laboratory of Molecular Biology, Hills Road, Cambridge CB2 0QH, UK.
Tel.: +44 1223 252969; Fax: +44 1223 213556;
E-mail: jyl@mrc-lmb.cam.ac.uk

**Received: 27 May 2008; accepted: 7 July 2008; published online: 24 July 2008**

 

## Results

### *A C-terminal peptide of ParR mediates the interaction with ParM filaments*

We designed an assay to specifically test the interaction between the R1 ParR–*parC* complex and ParM filaments (Figure 1A and B). Biotinylated *parC* DNA was bound to magnetic streptavidin-coated beads. Purified ParR and ParM were added in the presence of nucleotide and the washed beads were run on a SDS–PAGE gel to test which components remained bound. A number of R1 ParR mutant proteins were constructed and purified, and tested for ParM interaction using this pull-down assay (Figure 1A). Point mutations in the DNA-binding N-terminal region (K5S and R6S) abolished interaction with *parC* DNA as expected and therefore ParM binding was not detected. Loss of DNA binding was confirmed using a DNA gel shift assay (data not shown) and was previously shown using pB171 ParR (Møller-Jensen *et al*, 2007). Two point mutations in the C-terminal domain (R78S and K83E) had no effect on either DNA binding or ParM interaction. Deletion of part (ParR 1–101) or all (ParR 1–84) of the disordered C-terminal domain had no effect on DNA binding but completely abolished ParM interaction, confirming that the C-terminal domain, which is unstructured at least in the absence of ParM (Møller-Jensen *et al*, 2007), is responsible for mediating the interaction with ParM filaments.

To further test these findings, a synthetic peptide was made consisting of the 33 C-terminal residues of ParR (84–117), and this was tested for inhibition of the ParM–ParR*C* interaction using the same pull-down assay (Figure 1C). At very high concentrations (675 μM, 100 × ParM), the peptide inhibited ParM polymerisation. This is likely to be due to nonspecific crowding effects as it was also observed with high concentrations of lysozyme (20 × molar concentration, not shown). When present at 10 × the molar concentration of ParM, polymerisation was not affected but interaction with ParR–*parC* was abolished. This suggests that the C-terminal peptide is competing for the same binding sites on the ParM filament as the C termini of the ParR–*parC* complex. Relatively high concentrations of peptide were required to observe this effect, likely due to a low affinity of the monomeric peptide for ParM. This is probably combined with a high number of binding sites for the C-terminal peptide all along the ParM filament. On the ParR–*parC* helix there are at least 20 ParR C-terminal tails present, producing a very high local concentration. Supporting our data is the finding that the C terminus of pSK41 ParR is involved in ParM binding (Schumacher *et al*, 2007).

### *The promoter region within R1 parC repeats does not affect ParM stabilisation*

The R1 centromere-like *parC* repeat domain is interrupted by the presence of a 39-bp stretch of DNA containing the −35 and −10 promoter regions for the co-transcription of downstream ParM and ParR. In contrast, some other type II plasmid systems comprise continuous *parC* repeats (Figure 2A). Given that the crystal structures predict a continuous binding of DNA around the outside of a ParR helix (Møller-Jensen *et al*, 2007; Schumacher *et al*, 2007), we wondered how the composition and length of the R1 promoter region would affect the interaction of the ParR–*parC* complex with ParM filaments. If the promoter region were included in ParR binding, it would be expected that a change in length would introduce a frameshift, which would in turn affect ParR binding. Using the same pull-down assay described above, we found that changes in the length and composition of the R1 promoter region had no effect on

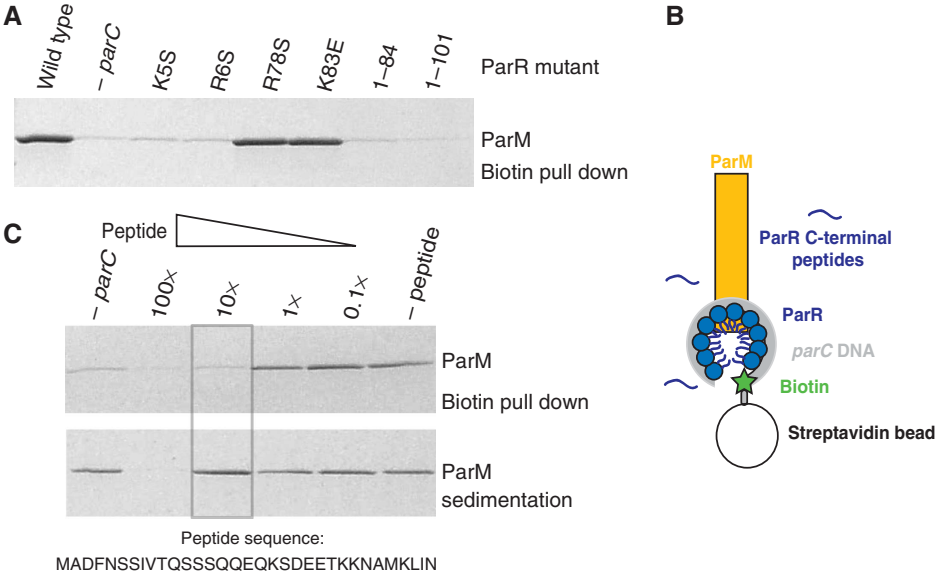


**Figure 1** The C-terminal peptides of ParR mediate interaction with ParM filaments. (**A**) Pull-down assay—purified ParM bound to streptavidin beads incubated with purified wild-type or mutant ParR. Mutants K5S and R6S are located in the DNA-binding part of ParR and abolish *parC* binding. Residues 78 and 83 are located in the C-terminal tail of ParR. Deleting the whole C-terminal region abolishes ParM binding (1–84 and 1–101). (**B**) Schematic drawing showing the pull-down assay used to test the interaction between ParM filaments and the ParR–*parC* complex. (**C**) A synthetic ParR C-terminal peptide (residues 84–117) interferes with ParR–ParM binding. Biotin pull down—purified ParM bound to *parC*-bound beads using wild-type ParR and decreasing amounts of C-terminal peptide. Polymerised ParM is detected using a sedimentation assay. The 33-residue ParR C-terminal peptide sequence used is given.

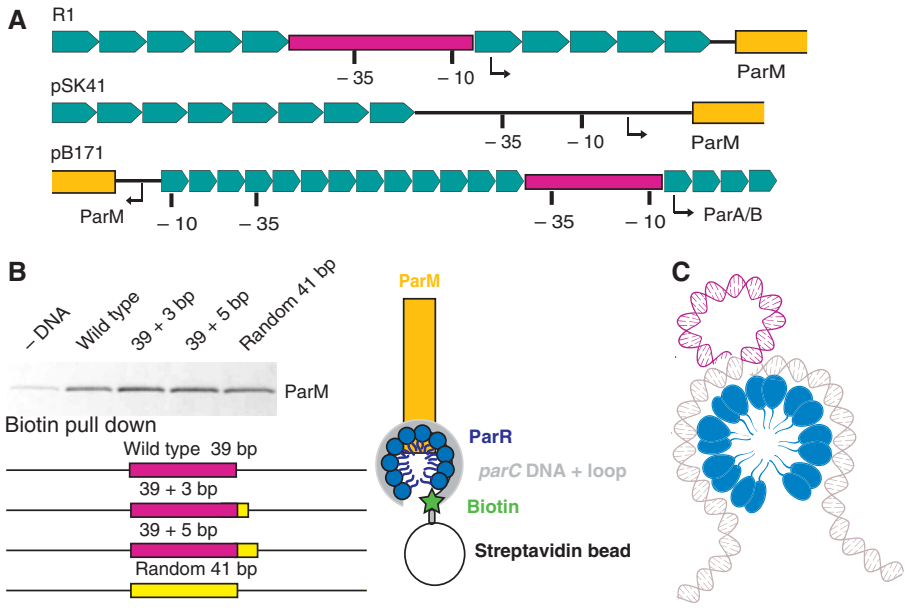


**Figure 2** The promoter region within the R1 *parC* domain does not affect interaction of the ParR–*parC* complex with ParM filaments. (**A**) Comparison of the *parC* domains of R1, pSK41 and pB171. R1 and pB171 contain interruptions in the *parC* repeats by regions containing promoters for downstream genes. (**B**) Biotin pull-down assay showing that changes in length and composition of the R1 promoter region do not affect ParM interaction. (**C**) Schematic drawing showing the proposed looping out of the promoter region when unmodified *parC* DNA binds around ParR. Promoter regions within *parC* repeats are shown in magenta and *parC* repeats in teal.

ParR binding or ParM interaction (Figure 2B). These results, together with the observation that other *parC* regions contain no such interruptions, lead us to the conclusion that the promoter region forms a DNA loop that protrudes out of the ParR-binding ring (Figure 2C). The loop is likely to perform a regulatory role in the transcription of R1 ParM and ParR and is consistent with the necessity for genomic efficiency of plasmids.

### *The ParR–parC complex binds to the ends of single ParM protofilaments*

Binding of ParR–*parC* to the ends of ParM filaments has been shown only indirectly by co-labelling plasmids and filaments *in vivo* (Møller-Jensen *et al*, 2003) and by using bulk *in vitro* assays (Garner *et al*, 2007). It has not been shown further whether each ParR*C* complex, formed on one plasmid, stabilises the ends of one or of several ParM filaments as each ParR*C* helix contains many C-terminal ParM-interacting peptides. We attempted to address these questions at the single-molecule level by using gold-labelled negative-stain electron microscopy. ParR was titrated against *parC* DNA using a DNA gel-shift assay, to determine the exact saturating concentrations where all DNA-binding sites are filled (Figure 3A). Similarly, gold-conjugated streptavidin was titrated against biotinylated *parC* DNA until all DNA molecules were labelled (Figure 3A). ParM was used at concentrations below which filaments form spontaneously in the presence of ATP, to ensure that any filaments observed were stabilised by the ParR*C* complex (Figure 3B). Negative stain electron microscopic analysis clearly showed gold-labelled DNA at the ends of single filaments (Figure 3C–P), and three conclusions can be drawn from these results. First, each ParR*C* complex binds to the end of a single ParM filament. Bundles of filaments emanating from a single gold label would be expected if each of the 20 ParR C-terminal tails bound a single ParM filament, and this was never observed. Pairing of labelled ends was sometimes seen (Figure 3P) and this could be explained by two *parC* DNA molecules being shared by two ParR rings. Such plasmid pairing has previously been observed *in vitro* (Jensen *et al*, 1998) and is likely due to the oligomeric nature both of the ParR protein and its binding sites on the DNA.

The second conclusion from these results is that the ParR*C* complex is able to bind simultaneously to both ends of a single, polar ParM filament (Figure 3O and Q). This was quantified by counting the number of filaments with 0, 1 or 2 ends labelled both in the presence of ATP and AMP-PNP. The overall labelling efficiency was relatively low, with 48% (ATP) or 37% (AMP-PNP) of filaments not labelled at either end. Despite this, double-labelled filaments could be observed in 6% (ATP) or 16% (AMP-PNP) of filaments. Therefore, unlike all known actin-binding proteins, the ParR*C* complex appears able, at least *in vitro*, to bind simultaneously to two non-identical ends of the ParM filament.

The third observation relates to the cause of end binding versus binding along the filaments. ParM is stabilised by an ATP cap at both ends, which protects the filament from disassembly (Garner *et al*, 2004). Given that ParR*C* binds to the ends of filaments, it is likely that the complex has a higher affinity for the ATP-bound ParM that predominates at the caps than ADP-bound ParM within the filament. To test this prediction, ParM filaments were assembled at high concentrations (125 μM) in the presence of either ADP or ATP and tested for both polymerisation and interaction with ParR*C* (Figure 3R). As predicted, ADP-ParM filaments assembled above their critical concentration did not interact with ParR*C* as tested using the pull-down assay (Figure 3R), in contrast to those assembled with ATP. ParR*C* binding along the filament could sometimes be observed (Figure 3N) and it would be

 

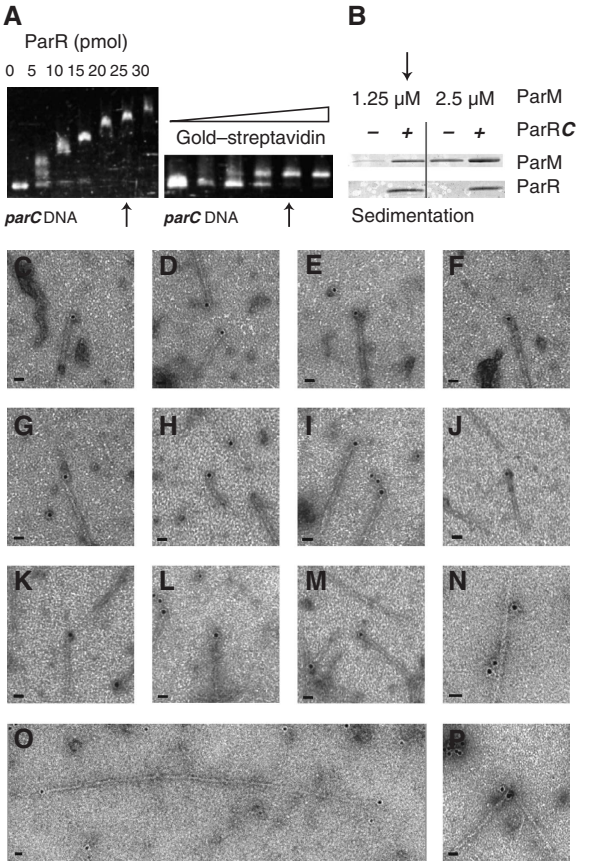


**Q**

| | Total filaments | Ends 0 (%) | Ends 1 (%) | Ends 2 (%) | Average complexes binding along filament |
|---|---|---|---|---|---|
| ATP | 166 | 48 | 46 | 6 | 0.17 |
| AMP-PNP | 120 | 37 | 48 | 16 | 0.83 |

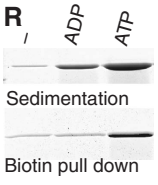


**Figure 3** Gold-labelled *parC* DNA binds as a ParR–*parC* complex to the ends of single ParM filaments. (**A**) Titration experiments to determine the optimal ParR and gold–streptavidin concentrations in relation to the amount of *parC* DNA used. Arrows indicate concentrations subsequently used. (**B**) Determination of the correct ParM concentration for the labelling experiment to minimise spontaneous filament formation in the absence of ParR*C*. (**C**–**P**) Electron micrographs showing ATP-polymerised ParM filaments with gold particles at the ends. ParR–*parC* complexes could also be observed binding along filaments (N) and complexes sometimes caused pairing of filaments (P). Scale bar 20 nm. (**Q**) Table quantifying binding events for ATP- and AMP-PNP-assembled filaments. Filaments were randomly imaged and classified as being gold-labelled at 0, 1 or both ends. The total number of side-binding events was counted and divided by the total number of filaments to give average number of complexes bound along the side per filament. (**R**) ADP-polymerised ParM (125 μM) does not interact with ParR*C* complexes as detected by the biotin pull-down assay. Polymerisation was tested using the sedimentation assay.

expected that this is a more frequent event with AMP-PNP-assembled filaments where the conformation of ParM within the filament would resemble that of the ATP cap. The number of side-binding events was quantified for both ATP- and AMP-PNP-assembled filaments. The average number of complexes binding along filaments was 0.17 in ATP-assembled filaments where the subunits within the filament would be in the ADP conformation, compared with 0.83 in AMP-PNP-assembled filaments. Taken together, these results suggest that the ParR*C* complex has a higher affinity for ATP-bound ParM, which is found at both caps of the filament, and that this at least partly leads to end binding of the complex. The exact mechanism underlying this difference in affinity is difficult to predict, as the conformation of polymerised ADP-ParM and ATP-ParM is unknown.

### *The ParR–parC complex interacts with the outside loop regions of ParM*

We next set about to identify the interaction site of the ParR*C* complex on ParM. For this, a peptide array was used to identify regions on ParM that interact with ParR*C* (Figure 4A). The peptide array displayed 60 partially overlapping peptides of 20 amino acids in length. The array was probed using a ParR*C* complex in which the DNA was both biotinylated and FITC-conjugated at opposite ends (Figure 4B). To enhance the signal both anti-FITC and FITC-conjugated anti-biotin antibodies were used, and further probed using FITC-conjugated secondary antibodies. Despite this enhancement the signal remained rather weak, probably due to the fact that the interaction is usually multimeric and distributed over larger parts of the ParM structure than tested here with unstructured 20-mers. The array was repeated five times, and the same two spots identified in each case (Figure 4A). The two spots, A8 and C12, correspond to regions 21–40 and 121–140 (Figure 4F), which each cover either partially or completely a loop region in subdomain IB of ParM (Figure 4D). Interestingly, these loops are smaller and different in both actin and the bacterial chromosomally encoded actin homologue MreB, supporting the assertion that these regions are involved in the ParR*C* interaction (van den Ent *et al*, 2002).

To verify and test this interaction further, 14 single-point mutations were designed based within the two regions of ParM identified by the peptide array. All 14 mutants were purified and tested both for polymerisation using a sedimentation assay, and for ParR*C* interaction using the pull-down assay described above (Figure 4C). Four mutants, K33A, R34G, W36A and F40A, exhibited a complete loss of polymerisation, and a further five, R127A, K128A, T131A, N133A and D136A showed an increase in the critical concentration required for polymerisation (not shown). This is likely to be due to the fact that the loop regions are also involved in forming contacts in filamentous ParM. Residues K33, R34, W36 and F40 may still be involved in ParR*C* interaction but the complete loss of polymerisation makes this difficult to test. One mutant was identified, which had the interesting phenotype where polymerisation was not affected but interaction with the ParR*C* complex was completely abolished. This residue, K123, faces outwards from helix 4 (van den Ent *et al*, 2002) just below loop 2 (Figure 4F–H). To test for smaller decreases in affinity, which would not be detected by the biotin pull-down assay, ParMs were polymerised below their critical concentration both in the presence and absence of ParR*C* (Figure 4E). In comparison with wild type and A124S, the addition of ParR*C* did not stimulate polymerisation of mutants S39A, R121A and K129A as expected for a loss of affinity. R121 lies close behind K123. S39 and K129 lie on the two loops 1 and 2 (Figure 4F–H).

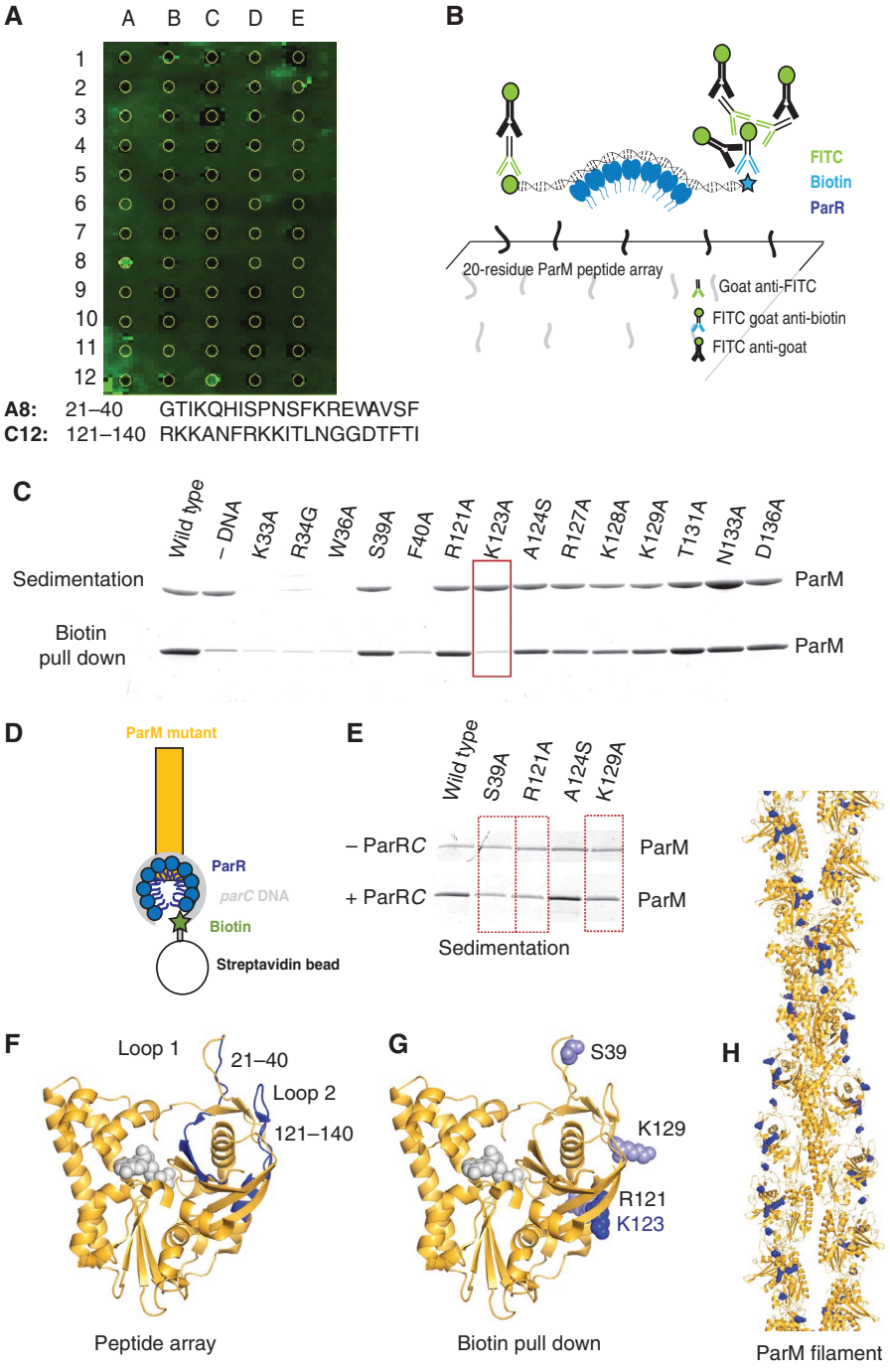


**Figure 4** ParR–*parC* binds to the outside loops of domain I of ParM. (**A**) Peptide array showing positive interactions between ParR–*parC* and ParM peptides, detected using FITC fluorescence. Positives are A8 and C12. (**B**) Schematic drawing showing use of a peptide array to identify the interaction between ParR–*parC* and 20-residue stretches of ParM displayed on a glass slide with double immuno-detection. (**C**) Biotin pull-down and sedimentation assay of purified ParM proteins carrying single-point mutations in regions identified by the peptide array. (**D**) Schematic drawing of the assay used. (**E**) Sedimentation assays testing the effect of ParR*C* on polymerisation of ParM below its critical concentration. ParR*C* no longer stimulates polymerisation of highlighted mutants. (**F**) Regions of ParM interacting with ParR–*parC* identified in the peptide array (dark blue). (**G**) K123 is strongly required for interaction with ParR–*parC* as identified using the biotin pull down of purified ParM point mutants (dark blue), and S39, R121 and K129 are weakly required as shown using the ParR*C* sedimentation assay (light blue). ADP is shown in white. (**H**) The interacting residues shown on a model of the ParM double helix. The residues lie on the outside of the helix.

### *ParRC forms a clamp that stabilises the end of growing ParM filaments*

We used negative-stain electron microscopy to visualise the unlabelled complex of ParRC-capped ParM filaments. DNA gel-shift assays were used to determine the concentration at which all *parC* DNA are bound by ParR (data not shown), and this ParR*C* complex was added to ParM below its critical concentration, in the presence of ATP. Under these conditions, rings of roughly 20 nm diameter could be observed sitting at the ends of ParM filaments (Figure 5A–L). No such structures were observed on unbound ParM filaments (Figure 5M–Q), and the gold-labelling experiments support

 

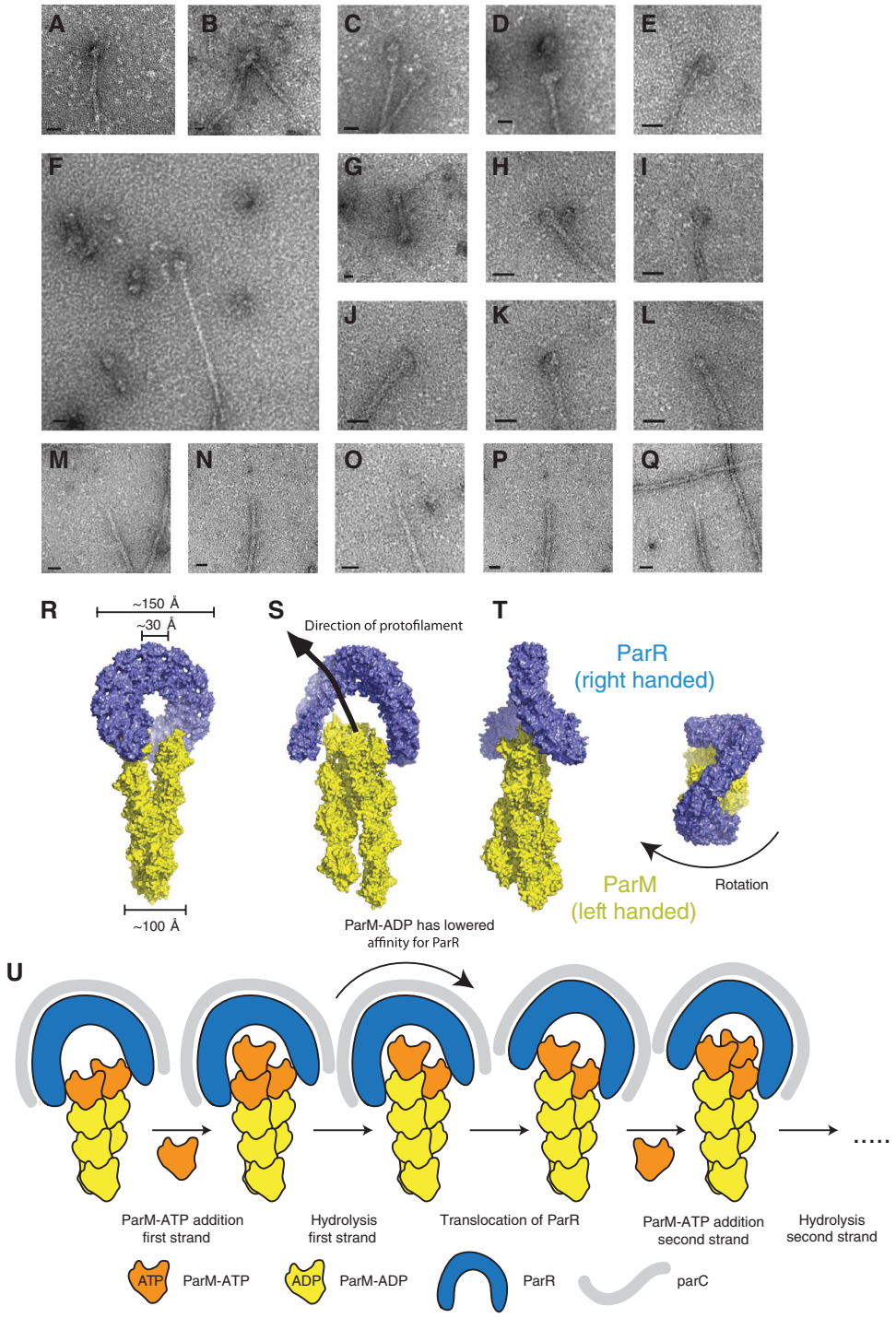


**Figure 5** The ParR*C* helix caps a single ParM double helical filament. (**A**–**L**) Negatively stained complexes of ParR*C*-capped ParM filaments. Despite its small dimensions (ParR helix 170 Å across from the crystal structure) a round structure can be seen at the end of many filaments. (**M**–**Q**) Negatively stained uncapped ParM filaments. (**R**–**T**) A model using the ParM filament structure and the ParR helix crystal structure (PDB code 1MWM) that we believe describes the images in (A–L) best. An end-on view shows the expected rotation as the complex polymerises through the cell. (**U**) Schematic drawing describing the processive ParM polymerisation mechanism derived from the structural model in R–T. The ParR*C* clamp binds to the two terminal ParM-ATP subunits and allows addition of one subunit to one protofilament at a time because of steric constraints. Hydrolysis of ATP to ADP releases the ParR*C* helix on one side only (causing processivity) and re-attaches to the newly added subunit, causing translocation. The re-attachment causes the ParR*C* helix to 'rock' and to allow addition of a new subunit to the second protofilament in exactly the same way.

the assertion that these rings are composed of ParR*C*. Furthermore, the dimensions of the rings match those of the ParR*C* complex shown previously by electron microscopy and X-ray crystallography in the absence of ParM (Møller-Jensen *et al*, 2007; Schumacher *et al*, 2007).

Guided by these observations and by the biochemical ParR–ParM interaction data shown here, the known crystal structure of helically packed pB171 ParR (Møller-Jensen *et al*, 2007) was modelled onto the end of the two-start left-handed R1 ParM filament (Figure 5R–T) (van den Ent *et al*, 2002;

Popp *et al*, 2008). The rise of the pB171 ParR helix is 13 nm and this opening forms a structure that neatly clamps the end of the ParM filament. Rotation of this ParMR*C* complex reveals views similar to those observed by electron microscopy (Figure 5A–L). The space between the ParR*C* clamp and ParM filament is filled by the ParR C termini, which were disordered in the X-ray structure and which we propose become ordered when binding to the ParM filament at the site determined above.

## Discussion

The data presented here lead us to a model for how DNA-coated ParR rings clamp and thus stabilise growing ParM filaments. The small DNA-binding ParR protein efficiently performs three distinct functions, which are all required to stabilise ParM. First, the N-terminal domain of ParR binds the pseudo-palindromic *parC* repeats through its $RHH_2$ fold in a sequence-specific manner. In so doing, it exerts an effect as a transcriptional repressor both for ParM and for itself. Second, the N-terminal domain is required to construct a rigid protein–DNA scaffold in the form of a large helix with the DNA wrapped around the outside. The formation of this scaffold appears to be an intrinsic property of oligomeric N-terminal ParR: the pSK41 ParR was crystallised in the absence of the C-terminal ParR domain (Schumacher *et al*, 2007) and the pB171 ParR was crystallised in the absence of DNA (Møller-Jensen *et al*, 2007). In both cases, the protein packed as the characteristic helix. It is therefore very likely that the *parC* DNA mainly serves to oligomerise ParR in the cell where concentrations would not be high enough to spontaneously form helices. The role of the DNA-nucleated N-terminal ParR helix is to form a rigid clamp, which wraps around the end of elongating ParM filaments. This way the ParR protein produces a structure with two-fold symmetry that matches the two-fold symmetry of the ParM double-helical filament. The third role of the ParR protein is the specific interaction of the C termini tails with the outside of ParM filaments. The affinity of this interaction is probably low, and facilitated by high local concentrations of ParR.

The handedness of both ParM filaments and the ParR*C* helix are critical for our model. It has recently been shown that ParM assembles into left-handed filaments (Orlova *et al*, 2007; Popp *et al*, 2008), which is the opposite orientation to F-actin. It is only in this conformation that new ParM subunits can access the ends of filaments capped with the right-handed ParR*C* ring as shown in Figure 5S and T.

Unlike actin and MreB, ParM assembles into a double-helical polar filament that exhibits equal growth at both ends (Garner *et al*, 2004). Our gold-labelling experiments show that the ParR*C* complex is able to bind to both ends of a single filament, and this raises the question of how two non-identical ends can interact with the same complex simultaneously. Our model potentially answers this question as the main stabilisation comes from the rigid clamp of the ParR*C* ring that can hold ParM filaments in either orientation by binding to the sides of the filament. The same loop regions on ParM will be accessible to the ParR C termini at both ends of the filament. This is supported by the observation that both in the gold-labelled and the unlabelled electron microscopy experiments, rings were sometimes observed binding along a filament (Figure 3N, not shown for unlabelled). This was observed much less frequently than the end binding, but indicates that the orientation of ParM relative to ParR*C* is not critical for binding. Given the equal rates of growth at both ends, and the ability of ParR*C* to bind in either orientation, we favour a model in which a single filament is attached to one plasmid at either end. However, an alternative model that we cannot rule out is that in the cell the filaments are actually composed of antiparallel bundles, with each pair of filaments bound to one pair of plasmids. In this case, ParR*C* would always bind to the same end of the polar ParM filament.

The geometrical model of the ParM–ParR interaction introduced here invites some speculation about the mechanism. A possible processive mechanism of ParR-induced ParM polymerisation and ATP-driven ParR translocation is outlined in Figure 5U. The ParR and ParM mutagenesis and binding data show that the C-terminal tails of ParR bind to the outside residues in domain IA of ParM. Because of the staggered nature of the double-helical ParM filament, the ParR ring bound to the end will be slightly tilted. This tilt allows just enough space for the addition of a single ParM subunit without creating clashes. The binding of a new subunit induces ATP hydrolysis in the previous subunit of the protofilament, which is still holding on to ParR. ParM-ADP then has a lower affinity for ParR and detaches. ParR stays attached to the filament through the other ParM-ATP subunit at the end of the second protofilament, introducing processivity. After detaching, ParR rebinds at the freshly added ParM-ATP subunit and thus translocates. This is the only free ParM-ATP subunit in the filament. Re-binding tilts the ParR helix in the opposite direction to before, allowing the addition of another ParM-ATP subunit to the second protofilament. From here on, the cycle continues with hydrolysis, ParR translocation and subunit addition. The end result is a device that produces motive force by the controlled addition of subunits to the two protofilaments in an alternating manner while rocking of the ParR clamp to either side.

It has not escaped our attention that the processive mechanism proposed here for the action of ParR–*parC* to polymerise ParM filaments is analogous to the model proposed for formins and their mechanism of F-actin polymerisation (Goode and Eck, 2007), with the important difference that formins only bind to one of the polar ends of F-actin. To our knowledge, the structures of the proteins (ParR versus FH2 domains) and binding surfaces are different but the systems utilise common principles: both the ParR and formin complexes produce dimeric structures that cap the filament ends and are proposed to attach in an alternating manner to the ends of the two strands of the double-helical filaments, producing processive motion without detaching. For both systems, it is proposed that the subunits are added alternating, based on steric constraints, and that the motion proceeds in a 'stair-stepping' way with a step size of $0.5 \times \sim 5$ nm (the monomer repeat). Because the ParMR*C* and actin/formin systems achieve these principles with different subunit structures they may represent an example of convergent evolution and the machinery for assisted polymerisation of double helical actin filaments has been invented at least twice.

One important consequence of our model is the rotation introduced into the plasmid DNA as the filament polymerises through the cell. With a crossover distance of roughly 30 nm the growing ParM filament would undergo approximately 16 turns as it moves through a 500 nm half-cell. Viewing the

 

complex from above (Figure 5T), it is clear that this rotation will introduce significant torsional strain on the 100 kb plasmid as it moves through the cell. How the cell manages this effect remains to be understood and may involve the action of topoisomerases.

The question remains as to how many ParM filaments are involved in segregating plasmids in the cell. Our electron microscopy experiments show that each ParR*C* complex, formed on one plasmid, binds to the end of a single ParM filament. With a copy number of 4–6 this could lead to the formation of a small bundle of filaments in the crowded environment of the cell, which would move a number of plasmids within a cluster. This is in accordance with fluorescence microscopy observations, which show that the fluorescence generated by ParM filaments *in vivo* is too high to be explained by a single filament (Campbell and Mullins, 2007). It is also possible that ParR continues to wrap DNA non-specifically beyond the *parC* site and in doing so form further open helices that could bind to and stabilise more ParM filaments, although this has not been observed in earlier experiments using larger pieces of DNA (Møller-Jensen *et al*, 2007).

The results presented here immediately open some interesting questions for further study. In terms of the molecular mechanism, we would like to test our prediction that ParR–*parC*-bound ParM filaments elongate at the same rate at both ends, and to test the extent to which ParR*C* binding stimulates ATP hydrolysis. Furthermore, how many ParR C termini actually interact with ParM at once? Given that the C termini mediate the specific interaction with ParM filaments, would it be possible to mimic this interaction by building the C termini on a different scaffold? In terms of the cellular mechanism of plasmid partitioning, our data invite re-interpretation of earlier observations. Plasmid pairing has been shown *in vitro* (Jensen *et al*, 1998), and plasmids are known to move as clusters in the cell (Weitao *et al*, 2000; Pogliano *et al*, 2001; Møller-Jensen *et al*, 2003; Ebersbach and Gerdes, 2004; Campbell and Mullins, 2007). As in mitosis, it is likely that newly replicated plasmids are paired prior to separation and then moved apart in bulk. ParM localises within clusters before forming pole-to-pole filaments separating the plasmids (Møller-Jensen *et al*, 2002). It was previously thought that pairing within the clusters was achieved through ParR–*parC* interactions following replication (Møller-Jensen *et al*, 2003). Given our findings, it is difficult to imagine how this could be achieved whilst still causing localisation of ParM within plasmid clusters. Rather, if there were another mechanism for pairing and/or clustering, perhaps related to host-encoded plasmid replication factors, short ParM filaments could form between ParR*C* on linked plasmid pairs until such a time as the linkage were released and the plasmids could be pushed apart. Following segregation, the ParR*C* must be released from the ends of the filaments allowing the ParM to depolymerise. The cause for this is unknown, and could be related to a new round of replication displacing bound ParR from the DNA.

## Materials and methods

### *Plasmids*

Genes encoding R1 ParM (35.7 kDa) and R1 ParR (13.2 kDa) were cloned into vector pHis17 (B Miroux, personal communication) without the addition of any extra residues to generate plasmids pJSC1 and pJSC21. Point mutations in ParM and ParR, and C-terminal truncations of ParR were derived from pJSC1 and pJSC21 by PCR mutagenesis. Constructs containing mutations in the *parC* promoter region were derived from pMD330 (Dam and Gerdes, 1994), which contains the minimal *parC* region in pUC19, by PCR mutagenesis.

### *Protein expression and purification*

R1 ParM and ParR were expressed in *E. coli* BL21-AI cells (Invitrogen) and purified essentially as described previously (van den Ent *et al*, 2002; Møller-Jensen *et al*, 2007) except gel filtration was not performed on the ParM point mutants.

### *Biotin pull-down assay*

Primers SR14 and biotinylated SR15 were used to amplify a 383-bp region of DNA containing the *parC* region from pMD330 or its derivatives (Møller-Jensen *et al*, 2007). Streptavidin-coated magnetic beads (Dynabeads M-280; Dynal Biotech) were washed twice in polymerisation buffer (30 mM Tris–HCl, 100 mM KCl, 2 mM $MgCl_2$ pH 7.5) and resuspended directly in 50 μl of the PCR reaction. After 5 min incubation, the beads were washed and resuspended in 20 μl 5 μM ParR for 5–10 min. After washing, the beads were resuspended in 37 μl polymerisation buffer containing 2 mM AMP-PNP. ParM (3 μl) was added to a final concentration of 6.25 μM (for the ParR mutant and peptide inhibition assays) or 12.5 μM (for the ParM mutant assays) or 125 μM (for the ADP/ATP comparison assay), mixed and immediately separated. Beads were washed three times in 20 μl polymerisation buffer containing AMP-PNP, and the separated beads were run on an SDS–PAGE gel.

For the peptide inhibition assay, the 33 amino-acid (~3700 Da) C-terminal peptide of R1 ParR was synthesised (Sigma) and solubilised in 0.1 M ammonium bicarbonate to 20 mg/ml. In the pull-down assay, the peptide was added at the same time as 6.25 μM ParM at 675, 67.5, 6.75 or 0.67 μM.

### *ParM polymerisation assay*

ParM was mixed in a volume of 80 μl with polymerisation buffer and 2 mM AMP-PNP. ParM concentrations were the same as used for the biotin pull-down experiments. In the peptide inhibition assay, peptide was added at concentrations given above. For the ParR*C* polymerisation stimulation assay, ParM was used at 1.25, and 0.6 μM ParR was added together with 40 ng 383 bp *parC*. The reactions were centrifuged at 100 000 *g* in a Beckman TLA 100 rotor for 15 min. The supernatants were removed, pellets resuspended in 20 μl, and 10 μl run on an SDS–PAGE.

### *ParM peptide array*

In total, 60 partially overlapping peptides of 20 amino acids in length covering the entire sequence of ParM were spotted onto a glass slide (JPT Peptide Technologies GmbH). FITC-conjugated SR14 and biotinylated SR15 primers were used to amplify a 385-bp region of pMD330 containing the *parC* region (Møller-Jensen *et al*, 2007). A gel-shift assay was performed as described previously (Ringgaard *et al*, 2007) to determine the exact concentration of ParR that would saturate the 20 binding sites on *parC*. This ratio of FITC-biotinylated *parC* and ParR was pipetted onto the peptide array and incubated in a geneframe in the dark and at 4°C overnight. The array was washed five times for 5 min in filtered double distilled water, and incubated sequentially with FITC–anti-biotin (goat), anti-FITC (goat) and FITC–anti-goat. All incubations were performed for 1 h at room temperature in the dark, and washed five times in between. After the final rinses, the slide was dried under nitrogen gas and scanned with a pixel size of 25 μm using a Typhoon 8610 Imager (GE Healthcare).

### *Gold labelling and electron microscopy*

Biotinylated *parC* was generated from pMD330 by PCR using SR14 and biotinylated SR15, and purified by gel extraction (Qiagen). Colloidal gold-conjugated streptavidin (5 nm) (Invitrogen Alexa Fluor 5 nm gold-conjugated streptavidin) was titrated against *parC* DNA and analysed using a DNA gel-shift assay to determine the saturating concentration of streptavidin gold. The exact concentration of streptavidin gold was not known. Similarly, ParR was incubated with *parC* DNA in increasing amounts to determine the maximum concentration. DNA (1 ng) was incubated with 25 pmol ParR and gold-conjugated streptavidin in the presence of 1.25 μM

ParM and 2 mM ATP or AMP-PNP in polymerisation buffer for 1 min at room temperature, then immediately pipetted onto a glow-discharged carbon-coated grid. After 1 min, the sample was blotted away and negatively stained with 2% uranyl acetate.

For unlabelled ParMRC, the grids were prepared as above except shorter DNA was found to give cleaner images, and unconjugated primers were used to amplify just the 150 bp minimal *parC* region of DNA from pMD330.

Electron microscopy was performed at 80 kV using a Philips EM208 transmission electron microscope, or at 120 kV using a Tecnai12 electron microscope. Images were photographed at a magnification of $\times 50\,000$ or $\times 52\,000$ and negatives were scanned at 6 μm per pixel using an MRC-KZA scanner. For the quantification experiments, filaments were randomly imaged by using a CCD detector and classified as having 0, 1 or 2 ends labelled. The total number of complexes bound to the sides of filaments were counted and divided by the total number of filaments counted to give a mean score per filament.

### *Modelling*

The pB171 ParR structure was manually modelled onto R1 ParM left-handed filaments using PYMOL. The R1 ParM model was taken from van den Ent *et al* (2002) except the handedness of the filament was changed to left-handed and the atomic structure of ParM was re-fitted manually.

## Acknowledgements

We thank Kenn Gerdes, Simon Ringgaard and Jakob Møller-Jensen for kindly supplying plasmids and strains.

## References

Campbell CS, Mullins RD (2007) *In vivo* visualization of type II plasmid segregation: bacterial actin filaments pushing plasmids. *J Cell Biol* **179:** 1059–1066

Dam M, Gerdes K (1994) Partitioning of plasmid R1. Ten direct repeats flanking the parA promoter constitute a centromere-like partition site parC, that expresses incompatibility. *J Mol Biol* **236:** 1289–1298

Ebersbach G, Gerdes K (2004) Bacterial mitosis: partitioning protein ParA oscillates in spiral-shaped structures and positions plasmids at mid-cell. *Mol Microbiol* **52:** 385–398

Ebersbach G, Gerdes K (2005) Plasmid segregation mechanisms. *Annu Rev Genet* **39:** 453–479

Garner EC, Campbell CS, Mullins RD (2004) Dynamic instability in a DNA-segregating prokaryotic actin homolog. *Science* **306:** 1021–1025

Garner EC, Campbell CS, Weibel DB, Mullins RD (2007) Reconstitution of DNA segregation driven by assembly of a prokaryotic actin homolog. *Science* **315:** 1270–1274

Gerdes K, Molin S (1986) Partitioning of plasmid R1. Structural and functional analysis of the parA locus. *J Mol Biol* **190:** 269–279

Gerdes K, Møller-Jensen J, Bugge Jensen R (2000) Plasmid and chromosome partitioning: surprises from phylogeny. *Mol Microbiol* **37:** 455–466

Gerdes K, Møller-Jensen J, Ebersbach G, Kruse T, Nordström K (2004) Bacterial mitotic machineries. *Cell* **116:** 359–366

Ghosh SK, Hajra S, Paek A, Jayaram M (2006) Mechanisms for chromosome and plasmid segregation. *Annu Rev Biochem* **75:** 211–241

Goode BL, Eck MJ (2007) Mechanism and function of formins in the control of actin assembly. *Annu Rev Biochem* **76:** 593–627

Jensen RB, Lurz R, Gerdes K (1998) Mechanism of DNA segregation in prokaryotes: replicon pairing by *parC* of plasmid R1. *Proc Natl Acad Sci USA* **95:** 8550–8555

Møller-Jensen J, Borch J, Dam M, Jensen RB, Roepstorff P, Gerdes K (2003) Bacterial mitosis: ParM of plasmid R1 moves plasmid DNA by an actin-like insertional polymerization mechanism. *Mol Cell* **12:** 1477–1487

Møller-Jensen J, Jensen RB, Löwe J, Gerdes K (2002) Prokaryotic DNA segregation by an actin-like filament. *EMBO J* **21:** 3119–3127

Møller-Jensen J, Ringgaard S, Mercogliano CP, Gerdes K, Löwe J (2007) Structural analysis of the ParR/parC plasmid partition complex. *EMBO J* **26:** 4413–4422

Nordström K, Molin S, Aagaard-Hansen H (1980) Partitioning of plasmid R1 in *Escherichia coli*. I. Kinetics of loss of plasmid derivatives deleted of the par region. *Plasmid* **4:** 215–227

Orlova A, Garner EC, Galkin VE, Heuser J, Mullins RD, Egelman EH (2007) The structure of bacterial ParM filaments. *Nat Struct Mol Biol* **14:** 921–926

Pogliano J, Ho TQ, Zhong Z, Helinski DR (2001) Multicopy plasmids are clustered and localized in *Escherichia coli*. *Proc Natl Acad Sci USA* **98:** 4486–4491

Popp D, Narita A, Oda T, Fujisawa T, Matsuo H, Nitanai Y, Iwasa M, Maeda K, Onishi H, Maeda Y (2008) Molecular structure of the ParM polymer and the mechanism leading to its nucleotide-driven dynamic instability. *EMBO J* **27:** 570–579

Ringgaard S, Ebersbach G, Borch J, Gerdes K (2007) Regulatory cross-talk in the double par locus of plasmid pB171. *J Biol Chem* **282:** 3134–3145

Schumacher MA, Glover TC, Brzoska AJ, Jensen SO, Dunham TD, Skurray RA, Firth N (2007) Segrosome structure revealed by a complex of ParR with centromere DNA. *Nature* **450:** 1268–1271

Sherratt DJ (2003) Bacterial chromosome dynamics. *Science* **301:** 780–785

van den Ent F, Møller-Jensen J, Amos LA, Gerdes K, Löwe J (2002) F-actin-like filaments formed by plasmid segregation protein ParM. *EMBO J* **21:** 6935–6943

Weitao T, Dasgupta S, Nordström K (2000) Plasmid R1 is present as clusters in the cells of *Escherichia coli*. *Plasmid* **43:** 200–204

 